PRELIMINARY RESULTS FROM THE HEAVY IONS IN SPACE EXPERIMENT

James H. Adams, Jr. and Lorraine P. Beahm
E. O. Hulburt Center for Space Research
Code 4154, Naval Research Laboratory
Washington, DC 20375-5000
Phone: 202/767-2747, Fax: 202/767-6473

Allan J. Tylka
Universities Space Research Association
Code 4154, Naval Research Laboratory
Washington, DC 20375-5000
Phone: 202/767-2200, Fax: 202/767-6473

SUMMARY

The Heavy Ions In Space (HIIS) experiment has two primary objectives: (1) to measure the elemental composition of ultraheavy Galactic cosmic rays, beginning in the tin-barium region of the periodic table; and (2) to investigate heavy ions which arrive at LDEF below the geomagnetic cutoff, either because they are not fully stripped of electrons or because their source is within the magnetosphere. Both of these objectives have practical as well as astrophysical consequences. In particular, the high atomic number of the ultraheavy Galactic cosmic rays puts them among the most intensely ionizing particles in Nature. They are therefore capable of upsetting electronic components normally considered immune to such effects. The below-cutoff heavy ions are intensely ionizing because of their low velocity. They can be a significant source of microelectronic anomalies in low inclination orbits, where Earth's magnetic field protects satellites from most particles from interplanetary space. The HIIS results will lead to significantly improved estimates of the intensely ionizing radiation environment.

INTRODUCTION

The space radiation environment affects spacecraft in several ways. Cosmic rays and trapped particles are the major cause of spacecraft anomalies in digital microelectronic systems. These particles can even cause components to fail suddenly. Space radiation dose slowly degrades the performance of most electronic devices and is the factor which ultimately limits the operational life of a spacecraft. The radiation dose received by astronauts ultimately limits the duration of all manned missions and may constrain the extent of human exploration of space.

LDEF carried several cosmic ray experiments. Two of these experiments are HIIS and the Ultra Heavy Cosmic Ray Experiment (UHCRE)[1]. Figure 1 compares HIIS and UHCRE with previous and planned experiments to measure cosmic ray elemental abundances above nickel. UHCRE is the largest cosmic ray experiment of all; HIIS is exceeded only by UHCRE and the proposed Heavy Nuclei Collector (HNC), which may be launched by the year 2000. HIIS and UHCRE provide complementary measurements of the cosmic ray elemental abundances. Whereas UHCRE's larger area enables it to measure the very rarest cosmic rays (at atomic numbers Z > 65), HIIS will extend the measurements to lower atomic numbers in the range of Z = 45-65, where the primary UHCRE detectors are not sensitive.

HIIS and UHCRE are also complementary in another way. UHCRE was designed to detect only relativistic cosmic rays, whose energy is so high that they pass through the detector. HIIS, on the other hand, was designed also to measure lower energy ions which come to rest in the detector. Potential sources of such stopping ions are solar energetic particles, the anomalous component of cosmic rays, and trapped heavy ions. Figure 2 compares HIIS with other existing and planned instruments to detect stopping ions. HIIS is orders of magnitude larger than any of these and can therefore make an unequalled
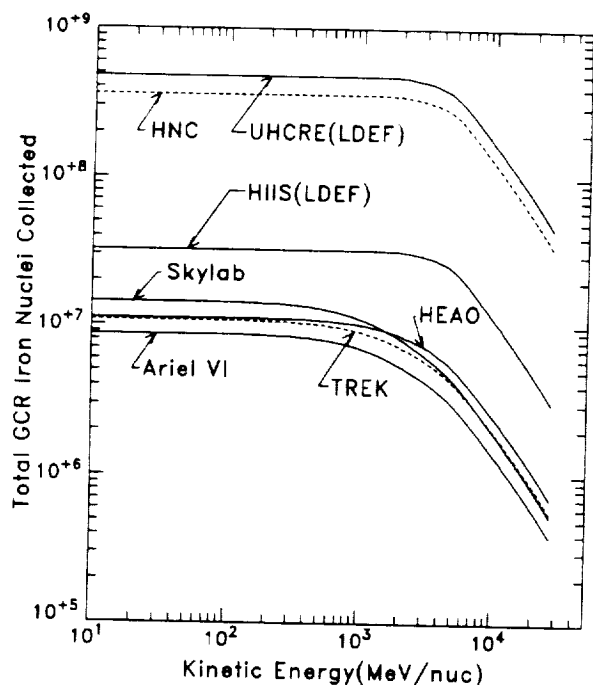
PRECEDING PAGE BLANK NOT FILMED

Figure 1: The collecting power of ultraheavy cosmic ray experiments, as measured by the total number of collected Galactic cosmic ray iron nuclei vs. minimum kinetic energy. In these comparisons, the effects of the different orbits are considered. Skylab[2], HEAO[3], ARIEL VI[4], HIIS, and UHCRE[1] (solid curves) have been flown. The TREK and HNC experiments (dashed curves) are planned for flight on the Soviet MIR and US Freedom space stations, respectively. The only flown experiment larger than HIIS is UHCRE. HIIS and UHCRE are complementary experiments, with HIIS ultraheavy measurements beginning at Z=45 and UHCRE's larger collecting power sensitive only to the rarest cosmic rays at Z>65.
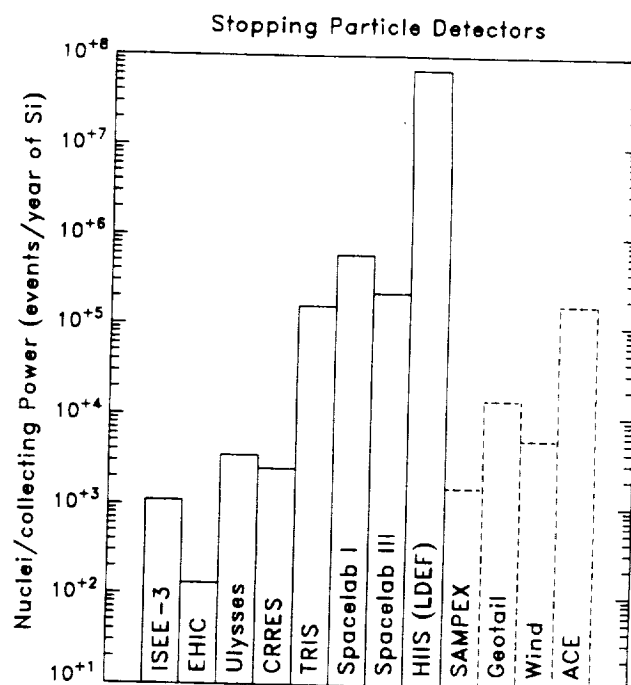
Figure 2: The collecting power of instruments which detect cosmic rays by bringing them to rest. The ISEE-3[5], CRIE/EHIC, Ulysses, CRRES[6], TRIS[7], Spacelab I[8], Spacelab III[9], and HIIS instruments (solid lines) have been flown. SAMPEX[10], Geotail[5], Wind[11], and ACE[5] (dashed lines) are planned for flight. The two spacelab missions and TRIS were flown less than a year, so for these missions the total number of Si events is plotted. Note that UHCRE[1] (Fig. 1) is not intended to detect stopping cosmic rays.

and extraordinarily deep survey of the stopping heavy ion contribution to the radiation environment. HIIS thus has the potential to make discoveries which may influence the direction of research and engineering for years to come.

EXPERIMENTAL OBJECTIVES

Ultraheavy Galactic Cosmic Rays. Galactic cosmic rays provide us with a sample of matter which originates from all over the Galaxy. We can use this sample to test our theory for the origin of the chemical elements. By comparing the composition of cosmic rays with that of the solar system and other samples of matter, we may discover differences that result from Galactic evolution over the past 5.5 billion years. These comparisons could also tell us about the special circumstances surrounding the formation of the sun and the solar system. The composition of the heaviest and rarest cosmic rays will be determined primarily by UHCRE. HIIS will contribute to the statistics of all ultraheavy cosmic ray measurements and it will extend observations down in atomic number to include the important tin-barium region of the periodic table, where we can observe the relative contributions of various nucleosynthetic processes[12].

Ions Below the Geomagnetic Cutoff. Satellites inside the magnetosphere are protected from many of the charged particles in the interplanetary medium because these particles are turned back by Earth's magnetic field. This was the case for LDEF, in its low altitude 28.5° orbit. The relevant quantity in measuring a particle's ability to penetrate into Earth's magnetic field is its magnetic rigidity, R, which is

simply the particle's momentum per unit charge. R is measured in units of GV/c, which is short for GeV/ec, where GeV/c is momentum in relativistic units and e is the charge in units of the electron charge. The minimum rigidity (ie, the so-called "geomagnetic cutoff rigidity") needed to reach the LDEF orbit is about 4 GV/c.

Because R is the momentum per unit charge, it depends upon both the particle's kinetic energy (K) and its charge (Q). Specifically,

$$R = (A/Q)[K^2 + 2KM_0]^{1/2} \tag{1}$$

where A is the ion's atomic mass number, $M_0 = 0.931$ GeV is the atomic mass unit, K is measured in GeV per nucleon (GeV/n), and Q is measured in units of the electron charge. Galactic cosmic rays are known to be fully stripped of electrons, so that Q = Z, where Z is the atomic number of the nucleus. In this case, the cutoff rigidity of 4 GV/c corresponds to a minimum kinetic energy of about 1 GeV/n. Particles which are detected at energies lower than this are said to be "below the cutoff". By definition, such particles must come from a source other than fully stripped Galactic cosmic rays.

Heavy ions trapped in Earth's magnetic field[13-15] are one source of below-cutoff ions. Another way for an ion to appear below the cutoff is if it has not been completely stripped of its electrons. In this case, Q < Z, thus giving the particle higher rigidity than a Galactic cosmic ray of the same energy. Compared to Galactic cosmic rays, such particles have enhanced access to low earth orbit. As discussed below, there are several known and possible sources of such particles. Because their relatively low velocities make these particles more intensely ionizing, they can be an important cause of satellite anomalies.

APPLICATIONS OF THE HIIS RESULTS

HIIS experiment will make a more thorough survey of the highly-ionizing particle radiation environment than has ever been possible before. We expect that the results of the HIIS experiment will lead to significant improvements in the Cosmic Ray Effects on Microelectronics (CREME) model[16-19]. CREME is widely used at present to estimate single event effect (SEE) rates on spacecraft. We anticipate that CREME will also be useful in designing the Space Station and in estimating radiation exposure to humans and hardware on future missions to the moon and to Mars. The results offered by HIIS and UHCRE cannot be duplicated by any existing or planned experiment within the next decade. These two LDEF experiments thus offer a unique and timely opportunity to increase our knowledge of the space radiation environment.

At present we can identify four areas in which the HIIS data will make CREME more accurate and improve its predictive capability:

1. *Ultraheavy Galactic Cosmic Rays*: Because these ions have such large nuclear charges, they are the most intensely ionizing particles in Nature. Although rare, these particles will affect microelectronic devices that are immune to the effects of more common cosmic rays. An accurate estimate of the flux of these particles is important in designing mission critical devices in which the mean-time-between-failures (MTBF) must be very large. HIIS and UHCRE will greatly reduce uncertainties in these flux estimates, particularly for the most intensely ionizing particles.

2. *Anomalous Component of Cosmic Rays*: These particles are known to be singly-ionized[7,20], which greatly increases their transmission through Earth's magnetic field to satellites in low-altitude, low-inclination orbits. In fact, anomalous component particles begin to dominate the linear energy transfer (LET) spectrum at LET values where many widely used electronic components become vulnerable. Current measurements of the anomalous component at Earth extend to only about 30 MeV/n for oxygen. These ions can be stopped by approximately 50 mils of aluminum shielding. At present we have only estimates of how the anomalous component spectrum extends to higher energies, where these ions can affect components behind typical amounts of shielding. HIIS will make the first high energy measurements of the anomalous component at Earth. HIIS
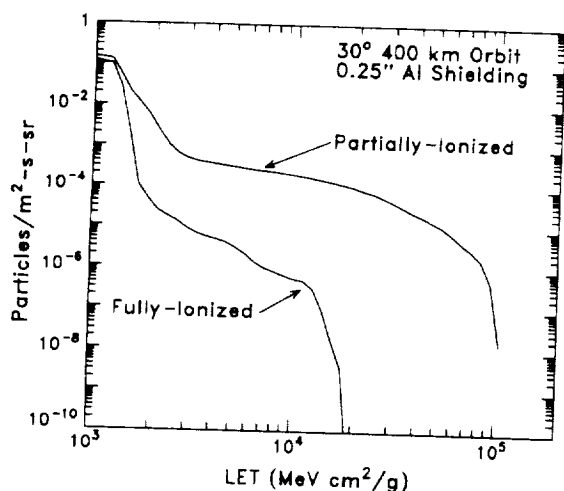
Figure 3: Linear energy transfer (LET) spectrum behind 0.25 in (0.64 cm) of aluminum for the peak particle flux of the August 1972 solar flares and as averaged around the Space Station orbit. Two possibilities are considered, that the solar energetic particles are fully ionized and that they are partially ionized as observed at low energies[21].
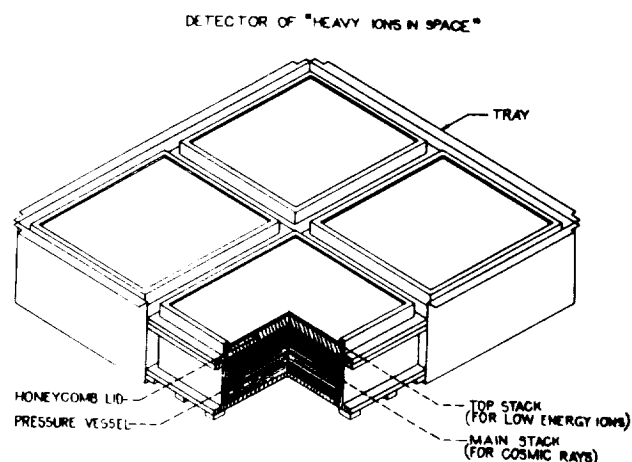

Figure 4: One of the two LDEF trays containing the HIIS experiment. Each tray contained four modules, one of which is shown in cutaway here.

will also measure heavier, more-intensely ionizing species in the anomalous component, whose contributions to the LET spectrum are presently unknown.

3. *Solar Energetic Particles (SEP)*: As discussed above, these ions can appear below the geomagnetic cutoff if they are less than fully stripped of electrons. Direct measurements[21] at low energies (~1 MeV/n) show that this is indeed the case, and indirect arguments[22] suggest that this behavior continues to energies of ~10 MeV/n. Particles of these energies can be stopped by modest amounts of shielding. At present there is no information on the ionization state of SEP's at very high energies of ~100 MeV/n. As shown in Figure 3, this lack of knowledge can lead to huge uncertainties in the radiation hazard posed by SEP events. Five large SEP events, which were also well measured on satellites outside the magnetosphere, occurred during the LDEF flight. By comparing the satellite measurements with the HIIS data, the ionization state of very high energy SEP particles can be deduced, thereby removing the uncertainties illustrated in Figure 3.

4. *Trapped Heavy Ions*: There is now good evidence for trapped oxygen ions with energies of 5-30 MeV/n in the inner magnetosphere[14]. Because LDEF was a 3-axis stabilized spacecraft, trapped heavy ions accumulate in HIIS at characteristic angles, thereby making them easily distinguishable from other particles. HIIS can extend the trapped particle measurements to higher energies and heavier species, making possible a first estimate of these particles' contribution to the satellite radiation environment.

Finally, we also note HIIS's potential to make new discoveries. For example, there have been recent published reports of below-cutoff ions which do not appear to be from any known source[23-25]. The collecting power of HIIS is orders of magnitude larger than that of the instruments which reported these results. HIIS should therefore be able to confirm (or refute) these observations and perhaps to identify the source of these particles. These particles, and others identified by HIIS, may be new and unanticipated components of the highly ionizing radiation environment.

THE HIIS DETECTOR SYSTEM

The HIIS detectors were contained in two trays (H3 and H12) on the space-facing end of LDEF. Each tray contained four modules. Figure 4 shows one of the HIIS trays and a cut-away of one of the modules. Each module comprised two separate stacks of plastic track detectors, a main stack which was sealed in

one atmosphere of dry air and a top stack which was in vacuum. Most of the sheets in the main stacks were CR-39[26], which was cast for us by Pershore Mouldings Ltd. (Pershore, UK) according to a special process for producing highly uniform, detector-quality material which we developed[27]. The top stacks and some sheets in the main stacks were Lexan[28]. The Lexan we used was manufactured especially for us without UV stabilizer, so as to make it possible to increase Lexan's sensitivity to lightly ionizing particles through UV enhancement of the latent tracks[29]. The total vertical thickness of the detector module was ~12 g/cm^2. The total number of detector sheets is 2782, each of which has an area of 1064 cm^2. The total collecting power of the eight detector modules is $A\Omega = 2.0$ m^2-sr.

Seven of our eight modules were constructed as described above. The eighth module had a special design to extend the detector's range to lower energies: both stacks were sealed in an atmosphere of dry air and the honeycomb lid shown in Fig. 4 was replaced with four thin Kapton[30] windows.

METHOD OF DETECTION

Plastic track detectors record charged particles by the trails of radiation damage they leave as they pass through the detector sheets. These tracks, which are revealed by chemically etching the detectors, are a permanent record of the particle's path and its rate of ionization in the plastic. The response of a plastic track detector is characterized by V_T/V_B, where V_T is the rate at which plastic is etched away along the damage trail and V_B is the rate at which bulk undamaged plastic is dissolved by the etchant. Because of radiation damage to the polymer $V_T/V_B > 1$, and the competition between V_T and V_B leads to the formation of a conically shaped etch pit whenever

$$(V_T/V_B) \cos(\theta) > 1 \tag{2}$$

where θ is the angle between the trajectory of the charged particle and the normal to the detector sheet[31]. V_T/V_B is empirically found to be an increasing function of the restricted energy loss[32] (REL), which provides a numerical measure of the radiation damage generally dependent upon Z, A, and the particle velocity, β. Etch pits are measured under a high precision microscope. From the displacement of etch pits on the bottom and top surfaces of a detector sheet, the incidence angle θ can be measured. V_T/V_B can be determined by measuring the dimensions of the etch pit[33,34].

Stopping ions are identified by following them to where they came to rest in the detector and by measuring V_T/V_B in each detector surface along the particle's trajectory. When these V_T/V_B values are plotted versus the distance to the end of the track (the so-called "residual range"), they fall upon characteristic curves determined by Z and A. Once the particle's identity is known, its total range in the detector specifies its incident energy.

For relativistic particles, REL (and hence V_T/V_B) is nearly constant as the particle traverses the detector. V_T/V_B can be precisely determined by averaging measurements from many detector surfaces. V_T/V_B depends primarily upon the atomic number Z and only very weakly upon the particle velocity β, so the average V_T/V_B value identifies Z even without a measurment of β.

POST-FLIGHT ASSESSMENT OF THE DETECTOR PERFORMANCE

CR-39 and Lexan track detectors have routinely demonstrated excellent charge resolution (on the order of ~0.15 charge units or less) in short-duration accelerator exposures of small detector stacks. In extended space-based exposures of large detectors, various environmental effects can degrade the detector performance. The HIIS apparatus was designed to minimize these effects, and most of our analysis since retrieval has been directed to assessing the actual impact of these factors on the performance of HIIS.

Thermal Analysis and Temperature Effects

The single most important factor affecting the charge resolution of track detectors is temperature. In fact, several early track detector experiments, which were flown before these temperature effects were fully understood, gave misleading results[35]. More recent experiments, which have recognized the importance of temperature control, have proven reliable (cf. Ref. 7). There are two ways in which temperature affects track detectors:

Registration Temperature Effect. The response of a plastic track detector to an ionizing particle depends upon the detector's temperature at the time of the particle's passage[36]. This registration temperature effect (RTE) has been measured extensively[36-39] in both CR-39 and Lexan. To approach the track detector's high intrinsic resolution, the detector's temperature must be kept within a limited range throughout its exposure.

To limit temperature variations within the HIIS detector stacks, the HIIS design included a passive thermal control system, in which surface materials, their thermal and optical properties, thermal connections to the LDEF spacecraft, etc., were all carefully chosen. These items were combined in a detailed thermal model of the apparatus, which used input temperatures at nodes on the LDEF spacecraft to predict the temperature variation in the detector stacks. The original HIIS design, combined with LDEF's pre-flight temperature specifications, yielded a target temperature range of -11 ± 3.5 °C. At this relatively cold temperature the RTE is less severe[38] and thermal annealing (see below) can be avoided.

Since the retrieval, we have repeated this thermal analysis. The LDEF program office has used temperature data recorded during the LDEF mission and detailed thermal modelling of the spacecraft to reconstruct the temperature history at various temperature sensors on the spacecraft[40]. One of these sensors was on the boundary of our trays, so we have an accurate record of temperatures of the LDEF structure to which our experiment was attached.

Using this record, variation in the solar illumination incidence angle, measurements of the absorptivity and emissivity (α/ε) of the various surfaces on and around HIIS, and a detailed thermal model of our experiment, we have simulated the temperature history of the main detector stacks. The results of the simulation, which are shown on the left in Figure 5, indicate that the temperature in the main stack was in the range of -7.5 ± 2.0 °C. This better-than-expected temperature stability is due to two factors. First, the LDEF spacecraft underwent a smaller range of temperature variations than predicted in the pre-flight analysis. Second, LDEF was warmest in those parts of the mission when HIIS received the least sunlight, thus making it possible for the HIIS passive thermal design to compensate for variation in the spacecraft temperature.

Part of the HIIS thermal control system failed at some point: the thermal blankets protecting the HIIS modules partially detached and rolled up, exposing parts of the top detector stacks to solar UV. The pattern of UV and atomic oxygen damage on the surfaces of the blankets suggests that the failures occurred late in the mission, perhaps when LDEF was at lower altitudes and vulnerable to atomic oxygen damage. The degree of blanket failure varied from module to module. Post-flight examination of the blankets revealed that the failures were due to shrinkage of the top face sheets, causing them to tear loose from the modules.

The blanket failure appears to have had relatively little impact on the temperatures of the main stacks: we repeated our thermal analysis, using degraded blankets and the measured α/ε of the exposed top-stack surfaces. The simulated temperature history of the main stacks after the blanket failure is also shown in Figure 5. Without the blanket, the main stacks were colder (average temperature -13.0 °C) and underwent a relatively larger range of temperatures (rms width 2.3 °C). The top detector stacks, which are used only in studying very low energy particles, were more severely affected. In retrospect, the temperature shift caused by the blanket failure is also understandable. First, the measured α/ε of the exposed Lexan surfaces nearly balanced solar heating and radiative cooling. The remaining imbalance was in the direction of cooling. Second, the top detector stacks, which consist of 25 layers of 5 mil Lexan, also acted as surrogate thermal blankets. On orbit photography shows that these exposed stacks billowed up,
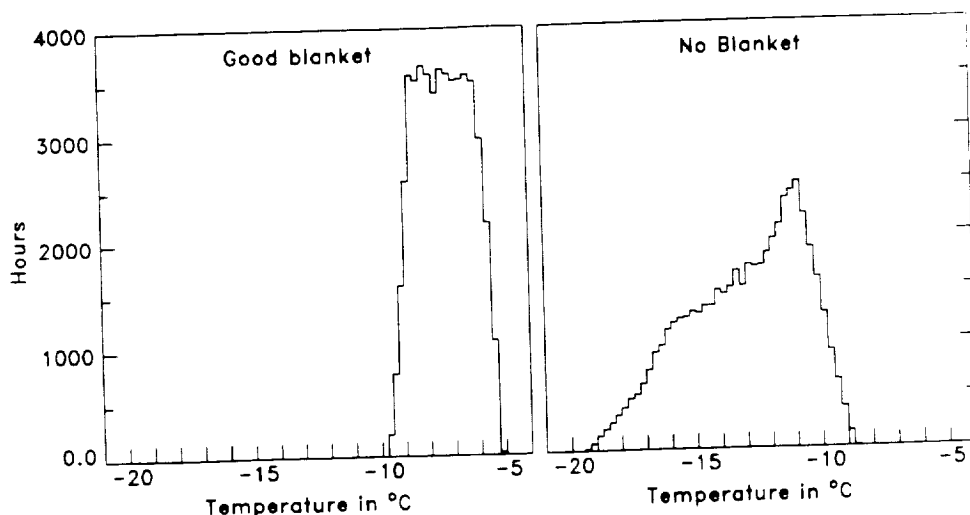
Figure 5: Post-flight reconstruction of the temperature distributions in the main detector stacks before and after the thermal blanket failures, which probably occurred near the end of the mission. Because we do not know exactly when the blankets failed, our simulations of thermal effects use the "worst-case" scenario, in which the blankets failed half-way through the mission, thereby producing the widest possible range of temperature variation.

probably due to electrostatic charging of the Lexan sheets by trapped electrons. With the sheets separated, heat transport through them was less effective.

The registration temperature effect will contribute to the widths of the elemental abundance peaks in the HIIS data. Although the post-flight examination of the blankets suggests that they failed near the end of the mission, we do not know this for certain. We therefore take a conservative approach in simulating the RTE on the detectors: we assume the "worst case" scenario, in which the blankets failed half-way through the mission, thereby averaging the histories in Figure 5 to produce the widest possible range of temperature variation. We folded this thermal history with results from accelerator studies of the RTE for particles with comparable V_T/V_B values. Even in this worst case, we find that the RTE is small: it increases the width of the Z=60 charge peak, for example, by less than 0.1 charge unit. For more heavily ionizing particles, the RTE is more severe: at Z=82, the RTE increases the width of the charge peak ~0.2 charge units.

Thermal Annealing. Thermal annealing[41] is the process in which radiation damage trails fade when the detector is held at elevated temperatures for extended periods of time after exposure. The HIIS modules were filled with dry air because measurements have shown that less thermal annealing occurs in dry air. Based on our post-flight thermal analysis and laboratory studies of thermal annealing, we conclude that the HIIS detectors remained too cool during the mission to be affected by annealing. From temperature sensors within our detector modules, which recorded the highest temperature to which they were ever exposed, we have independent verification that the temperatures in the main detector stacks never exceeded 37°C at any time since leaving our laboratory in 1984. Since retrieval, the HIIS detectors have been stored in refrigerators at ~5°C, except for ~2 months at ~20°C between retrieval and the return of the detectors to our laboratory.

Track Aging Effect

Another possible influence on the experimental charge resolution is track aging[42], in which the radiation damage continues to grow for a period of time after irradiation. Track aging has been a major concern for extended exposures of track detectors since the range of ages could degrade the charge resolution[43]. Recent experimental work[44], however, has shown that track growth occurs only in the first few weeks following exposure. Since the HIIS detectors are not etched until at least one year after the flight ended, this effect should not be present in our data.

Post-Flight Condition of the Detectors

The HIIS main detector stacks were originally sealed in 1 atm of dry air. The special module with the Kapton windows leaked because the windows were punctured by micrometeoroids after the thermal blanket rolled up. We analyzed the air in the remaining modules and compared it with air from the bottle used to fill the modules before flight. This air contained 10% helium as a tracer. The same helium concentration was found in the post-flight modules, proving that they did not leak. The analysis of the gas in the modules did, however, reveal a change in composition. The concentration of O_2 varied from module to module, with values in the range of 12-20% of the pre-flight concentration. Most of the O_2 had been replaced by carbon dioxide, but some was no longer in gaseous form. Oxygen is consumed during the polymerization process. The HIIS CR-39 was manufactured over a six month period, and some sheets were freshly polymerized when the modules were sealed. Since the detector sheets almost completely filled the module volume, residual polymerization of the CR-39 after the modules were sealed could easily account for the missing O_2 and the variation in the modules' O_2 concentrations. If residual polymerization is the explanation of the missing O_2, the oxygen concentrations probably leveled out to near their final value prior to launch.

After analyzing the gas in the detector modules, the main detector stacks were disassembled. We have etched sample sheets from the main stacks in two detector modules, C and E, in which the residual O_2 concentration was lowest and highest, respectively. Because chemical etching is an irreversible process and because we did not wish to lose valuable cosmic ray data, we first etched 10 sheets from near the bottoms of these modules. We also etched portions of a few sheets from near the top of the main stack in module C.

In all of the etched sheets, we easily found both relativistic and stopping cosmic ray tracks. The density of etch pits was not too high, and unrelated etch features did not interfere with measurements of the cosmic ray tracks. On the basis of our measurements of these tracks, we conclude that the main detector stacks, at least in the seven modules which did not leak, contain valuable cosmic ray data. Portions of the top stacks may also be useable for measuring fluxes of low energy particles, since they show no signs of UV exposure after the blanket failures.

CALIBRATION OF THE HIIS DETECTORS

We conducted extensive pre-flight accelerator calibrations of the HIIS detectors. Our present plan, however, is to internally calibrate the HIIS detectors, using the cosmic rays themselves. The detector sheets we have etched so far contained tracks, but not in the numbers we expected. Relativistic Fe, for example, appears not to have been recorded. Such apparent reduction in CR-39's sensitivity has been observed before[45]; it is consistent with the reduced oxygen concentration in the modules[46]. Because the observed detector response is so different from that in accelerator exposures, we believe that "boot-strapping" from the observed cosmic ray tracks is the most reliable calibration method. This method also ensures that the environmental effects on the HIIS detectors, whatever they may have been, will be reflected in the detector calibration.

To illustrate this internal calibration method, Figure 6 shows the raw data from stopping heavy ion tracks in CR-39 near the bottom of Module C. The data organize themselves into a densely populated band, labeled Fe, with a spread of tracks below the Fe band. There are only two ion tracks that are more intensely ionizing. This indicates a sudden drop in the elemental abundance of the ions. According to the general abundance of elements, there are only two places in the periodic table where such a drop occurs, above Fe and above Pb. Pb ions are far too rare to explain the observed fluxes, so the band must be Fe. Based on the number of ions in the Fe band, we would expect one or two Ni ions, just as observed. We therefore assumed that the heaviest ion track in the dataset was Ni. We then tried various hypotheses for the identity of the lightest track. When the lightest track was assumed to be Ar, the calculated Fe calibration curve ran through the Fe band. Using only the Ni and Ar measurements as input, we then derived the calibration curves for the other elements, also shown in Figure 6. In most cases we show
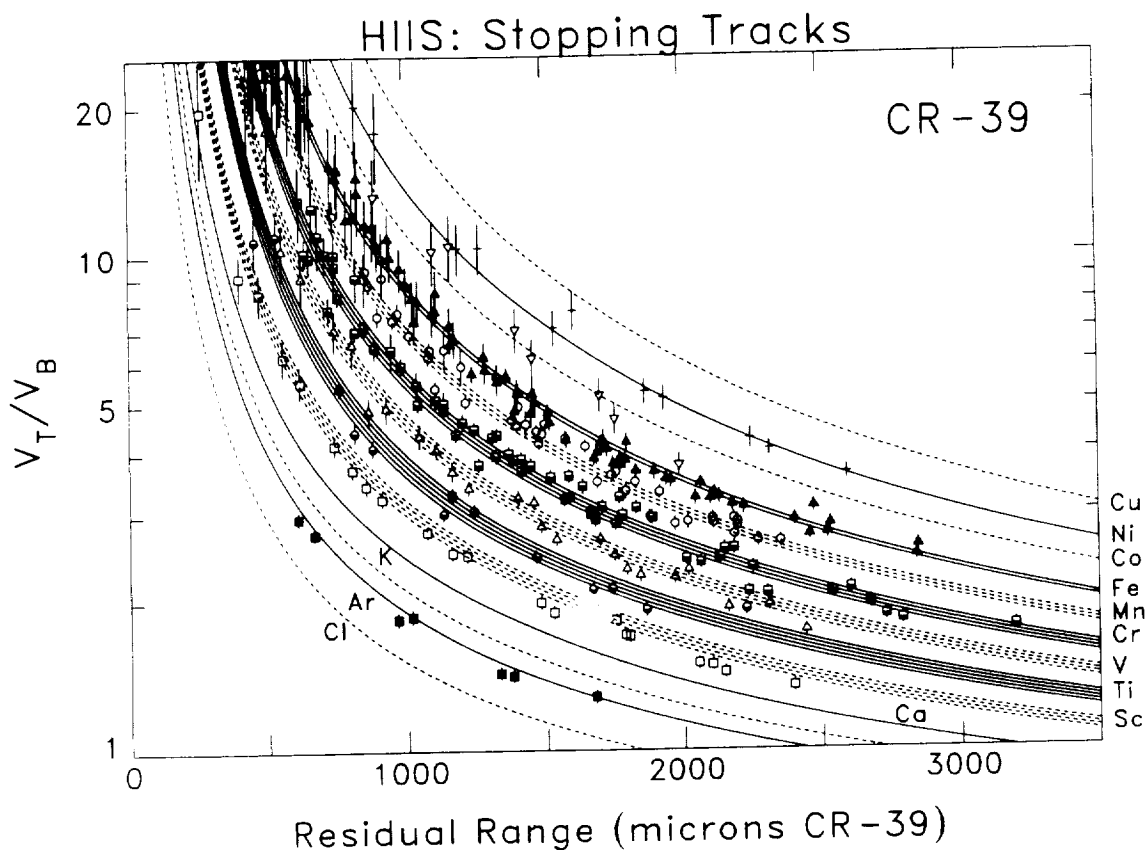
Figure 6: Raw data on 40 stopping heavy ion tracks found in detector sheets near the bottom of the main stack in Module C, each of which is measured in 9 detector surfaces on average. A different symbol is used for each element. The ordinates are the track detector response V_T/V_B and the abscissae are the distance from the stopping end of the track. The calibration curves are derived from the highest and lowest tracks shown in the figure.

curves for more than one isotope of each element. Because these ions were detected so deep in the stack, fragmentation guarantees that many isotopes are present. We have considered in our analysis only the most abundant isotopes, as indicated by a detailed calculation of transport through the detector material.

To apply the calibration, the measurements for each ion were fitted while leaving the atomic number as a free parameter. For atomic numbers with multiple isotopes, the Z/A ratio of the best-fit abundant isotope was assumed. The histogram of fitted Z values is shown in Figure 7. Most of the ions are unambiguously identified. This is illustrated in Figure 8, which shows how the "goodness of fit" (as measured by the integrated probability of the χ^2 distribution[47]) changes as the atomic number is moved up and down by one unit from the most probable integer value. The large sub-Fe to Fe ratio in Figure 7 may appear unusual. However, these tracks were found under ~15 g/cm^2 of material. Our transport calculation, combined with the Z-dependent geometry factor implicit in equation (2), shows that the observed sub-Fe/Fe ratio is consistent with an incident Fe beam.

To estimate the detector's charge resolution, we shifted all the elemental peaks in Figure 7 to overlay them at Z=26. Figure 9 shows the resulting distribution, which gives a good fit to a gaussian with standard deviation $\sigma = 0.19$ charge units.

The above internal calibration can be improved by collecting more tracks. Because the detector response varies from module to module, we will have to repeat the above process and do a separate
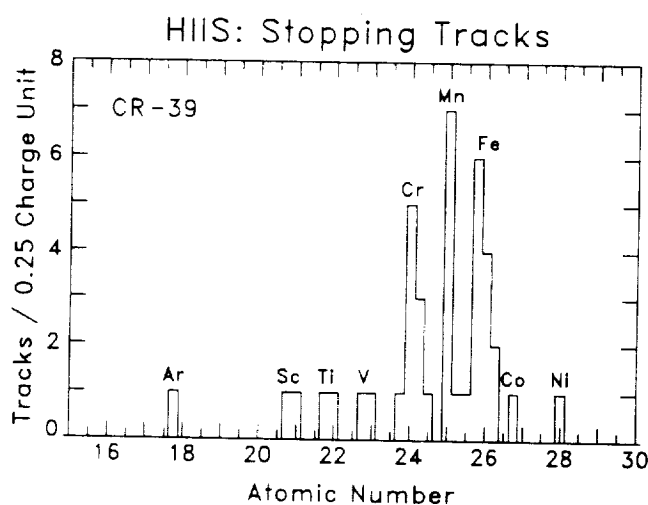
385

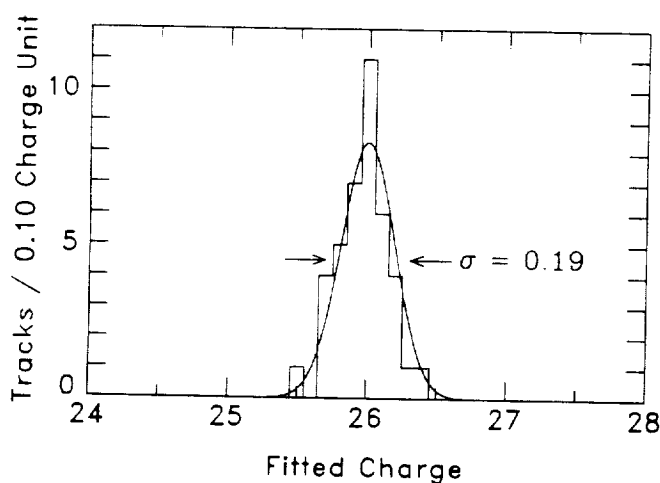Figure 7: Histogram of the fitted atomic numbers of the stopping ions.

Figure 8: Goodness of fit measures for the identified Z = 24, 25, and 26 tracks in Figure 6. The goodness of fit is measured by the probability of observing a worse χ^2 when fitting the track to the specified hypothesis (Zfit, Zfit-1, or Zfit+1, where Zfit is the most probable integer value of Z). The probability is calculated by integrating over the χ^2 distribution[47]. The plot shows that the fit probability generally drops sharply when moving up or down by one unit from the most probable Zfit value. This implies that the tracks are unambiguously identified.

Figure 9: The atomic number measurements from all the stopping tracks, scaled to overlay at 26. A gaussian fit to the distribution yields σ = 0.19 charge units.
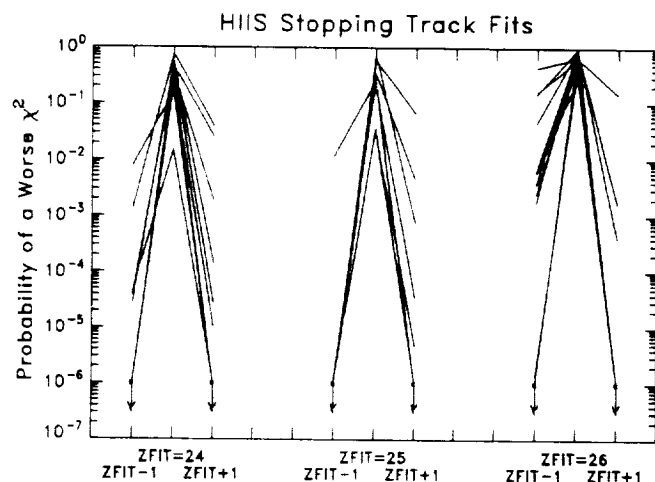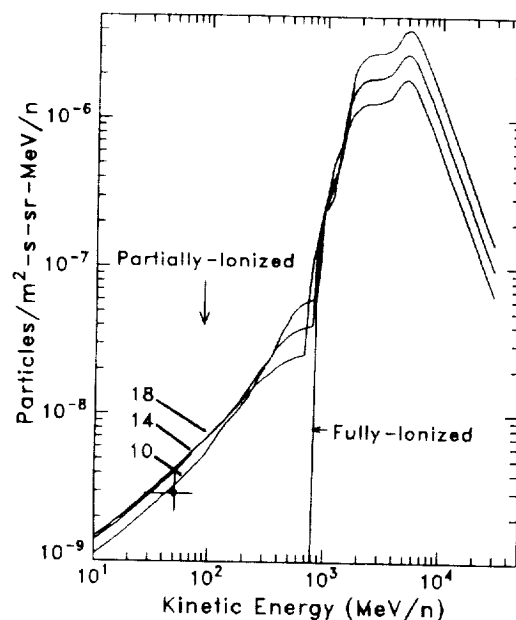

Figure 10: A comparison of the observed stopping Fe flux with estimates from solar energetic Fe ions with the same charge state distribution as observed at ~1 MeV/n. The spectra are the arriving Fe flux at depths of 10, 14, and 18 g/cm^2 in the HIIS detector stack. For comparison, we also show the spectrum for fully-stripped SEP Fe ions (which is not sensitive at low energies to the amount of material) under 14 g/cm^2. Galactic cosmic rays, which do not contribute to the low-energy flux, are also included in the calculations.

386

calibration for each module.* This should be no problem, since the necessary cosmic ray tracks appear to be present at the bottoms of the detector modules. Our thermal modelling indicates that the temperature in the main detector stack was uniform to within less than 0.3°C, so the calibration should be the same at both the top and bottom of a stack. The anomalous component Ne and Ar tracks, which we have already observed in the etched sheets near the top of the main stack in Module C, will provide another internal check on the calibration.

PRELIMINARY RESULTS ON STOPPING HEAVY IONS

The stopping heavy ions found near the bottoms of the stacks were a surprise: neither the anomalous component (because of its steeply falling spectrum) nor Galactic cosmic rays (which are geomagnetically excluded below ~1 GeV/n) are expected to stop at this depth in the stack. Based on the data collected so far, the average Fe flux under ~14 g/cm^2 is $(3\pm1)\times10^{-9}/m^2$-s-sr-MeV/n in the energy range $33 < E < 75$ MeV/n. These Fe ions arrived at LDEF with energies of ~600 MeV/n, much higher than previous observations of stopping ions. One possible source for these particles is re-entrant albedo of Galactic cosmic rays. We have performed numerical simulations which show that $18\pm6\%$ of the incident Galactic cosmic ray iron ions must scrape through the atmosphere to explain the observed flux. This appears to be far too much, so we have rejected this explanation.

Another possibility is that these particles come from the very large SEP events which occurred during the LDEF mission. At ~1 MeV/n, SEP Fe ions are known to be only partially-ionized[21], with a distribution of charge states with mean value of about 14. If this charge state distribution is independent of the energy, the SEP's might explain our stopping heavy ions.

Figure 10 on the previous page shows a first, crude attempt to test this explanation. To estimate the SEP Fe fluence during the LDEF mission, we multiplied proton fluxes measured on NOAA's GOES satellite in 1989 and 1990 by the average SEP Fe/proton ratio[48,49]. The combined Galactic and SEP Fe spectrum was then transmitted through the geomagnetic field to the LDEF orbit, assuming the SEP Fe nuclei to be either fully-ionized or partially ionized according to the charge state distribution observed at low energies. The flux was then propagated through the detector to various depths, corresponding to a range of incidence angles and consequent shielding thicknesses at the observation point. The crudeness of the SEP Fe flux estimate makes the calculated spectra in Figure 10 quite uncertain, but the results clearly suggest that partially ionized SEP's could explain the observed flux.

We plan to continue our investigation of stopping ions in the bottoms of the HIIS stacks. So far we have examined only ~1% of the sheets that would contain partially-ionized SEP ions. Based on the data so far, we expect ~1000 stopping Fe ions with incident energies between 350 and 900 MeV/n.

PLANNED ANALYSIS OF RELATIVISTIC ULTRAHEAVY GALACTIC COSMIC RAYS

Figure 11 illustrates our method for measuring ultraheavy Galactic cosmic rays. The figure shows the raw data for 13 relativistic tracks found in scanning part of a sheet near the bottom of Module C. The tracks were followed through 10 sheets, and V_T/V_B was independently measured in ~20 detector surfaces. The error bar on each V_T/V_B measurement is determined by propagating the measurement errors on the etch pit dimensions. The average value of V_T/V_B is determined to within ~1% precision. We have checked that the scatter of measurements around these mean values follows a normal gaussian distribution.

To identify the tracks, we used the CR-39 calibration derived from the stopping tracks, which cover the

*Analysis of stopping tracks at the bottom of the second module (Module E) is still in progress. Fluxes of stopping and relativistic ions in Module E are similar to those observed in the first module (Module C). The track detector in Module E seems to be somewhat more sensitive than that in Module C, consistent with E's higher residual O_2 concentration. This increased sensitivity may allow us to extend observations to lighter ions.

CR-39

V_T/V_B

0   1000   2000   3000   4000

Location (microns CR-39)

Fitted atomic numbers (right axis): 68.5 +/- 0.2, 67.1 +/- 0.2, 66.1 +/- 0.1, 64.7 +/- 0.1, 63.1 +/- 0.1, 62.5 +/- 0.1, 60.9 +/- 0.1, 58.8 +/- 0.1, 58.4 +/- 0.1, 56.6 +/- 0.1, 56.1 +/- 0.1, 55.2 +/- 0.1, 48.3 +/- 0.1
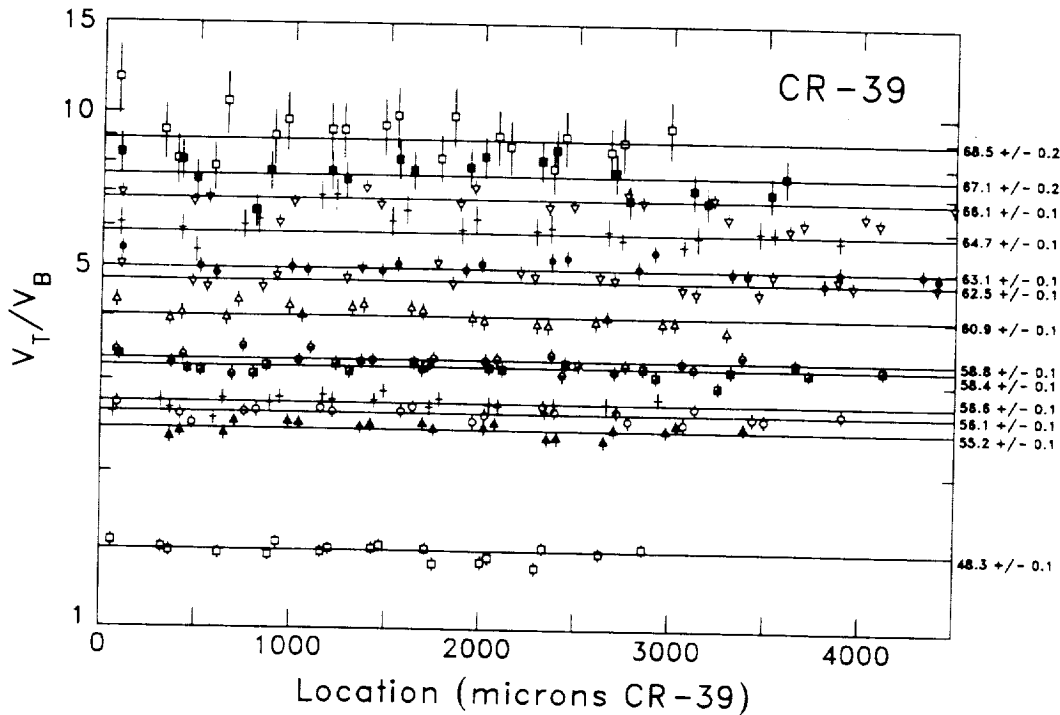
Figure 11: Raw data on relativistic tracks observed near the bottom of one HIIS detector stack. A different symbol is used for each track. The fitted atomic number and the formal error on the result are given at the right.

same range of V_T/V_B values. Figure 11 also shows the fitted atomic numbers, along with the formal error derived by propagating the uncertainty in the average value of V_T/V_B. Since these measurements were made under ~15 g/cm^2 of material, no strong elemental accumulations are expected. Also, although the formal errors are 0.1-0.2 charge units, the fitted atomic numbers do not tightly cluster around integer values. Temperature effects and uncertainties in the present calibration are too small to account for this spread in the fitted atomic numbers. Monte Carlo simulations of the HIIS resolution (discussed below) suggest that the primary reason for the spread is "kinetic smearing": the atomic numbers were fitted by assuming a particle energy of 11 GeV/n, but the actual particle energy can be anything above ~1 GeV/n. The detector response's residual weak dependence on the particle velocity combines with the Galactic cosmic ray spectrum to produce characteristic non-gaussian charge peaks. (These charge peaks are illustrated in Figure 12, discussed below.)

To measure elemental abundances of ultraheavy cosmic rays, we will apply the method shown in Figure 11 to tracks found in CR-39 and Lexan sheets near the tops of the main detector stacks. The tracks will be followed deeper into the stack and measured several more times to eliminate slowing down particles, which are a potential background for the heaviest and rarest cosmic rays.

Using previously reported relative abundances[3] and taking into account detection efficiency, geomagnetic transmission, and solar modulation of the Galactic cosmic ray flux throughout the LDEF flight, we expect to find a total of ~1500 relativistic cosmic rays at atomic numbers $Z \geq 45$ in the seven HIIS modules which did not leak. (For comparison, the HEAO dataset[3], which is currently the world's best data on the abundances of ultraheavy cosmic rays, contained ~370 such tracks.) After accounting for fragmentation losses, the number of tracks shown in Figure 11 is consistent with this flux estimate to within statistical errors.

To get an idea of the kind of composition measurements offered by HIIS, we have simulated the expected charge histogram. In this simulation we took into account: (1) the geomagnetic modulation of the cosmic ray flux and spectrum to LDEF's orbit; (2) the ultraheavy relative abundances[3,19]; (3) fragmentation in the ~2 g/cm^2 of material above the measured sheets; (4) the collecting area and exposure time of the seven HIIS modules that did not leak; (5) the detector calibration; (6) the Z-dependent
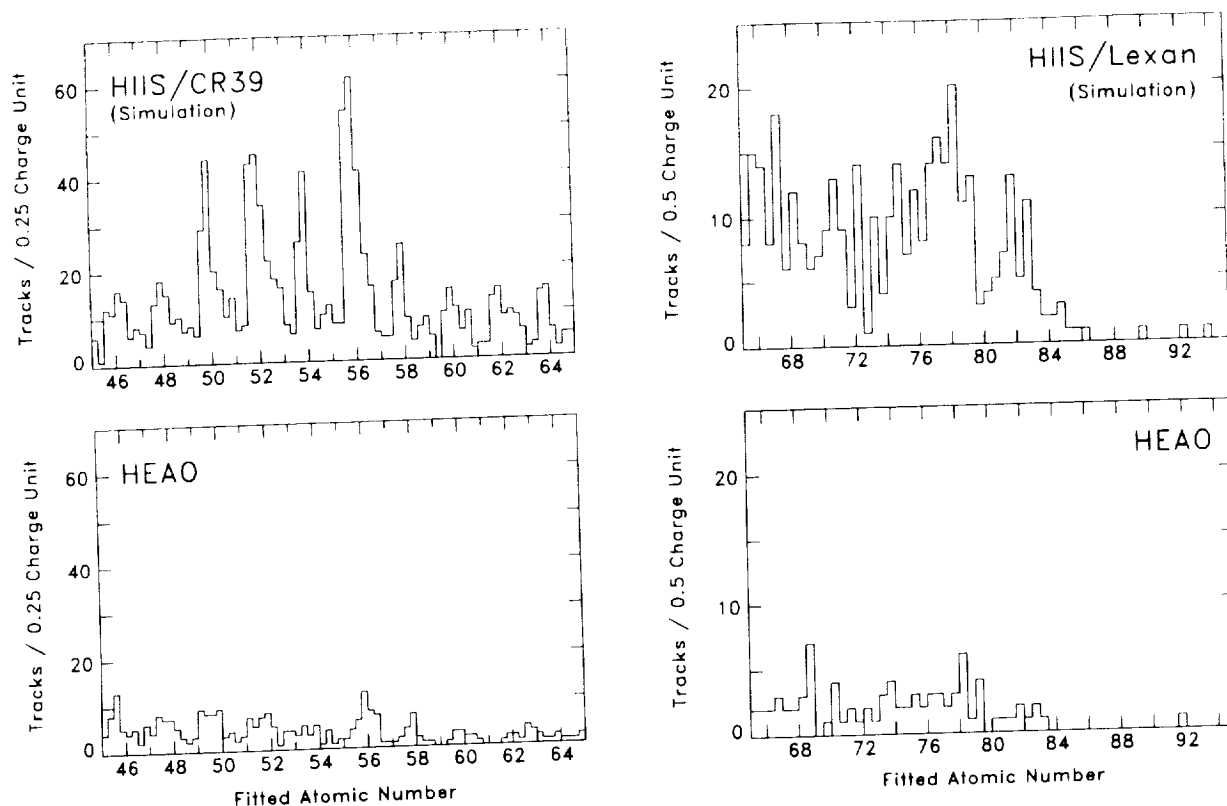
Figure 12: This figure compares the observed charge histogram from the HEAO experiment[3] with a simulation of the expected HIIS charge histogram. (See text for details of the simulation.) HIIS will primarily use CR-39 and Lexan detectors below and above $Z = 65$, respectively. The non-gaussian charge peaks caused by kinetic smearing are clearly seen in the $Z < 65$ simulation.

geometry factor implied by the detector response and equation (2); (7) kinetic smearing; (8) the registration temperature effect, based on our reconstruction of the thermal history of the detectors; and (9) measurement errors. Figure 12 compares the simulated HIIS measurements with the the HEAO data[3]. The simulation shows that HIIS offers a substantial improvement over the HEAO results. At $Z < 65$, HIIS will make more accurate measurements of the even-Z elements and, in some cases, the first abundance measurements of odd-Z elements. Above $Z = 65$ HIIS cannot resolve elements, but the Pt (Z=78) and Pb (Z=82) peaks are clearly separated. This is important because the Pt/Pb ratio is a key indicator of the nucleosynthetic processes which produce the cosmic rays.

CONCLUSIONS

The HIIS experiment has returned from its extended sojourn in space with valuable cosmic ray data covering a broad range of energies and atomic numbers. Our detailed review of environmental factors which affect plastic track detectors indicates that HIIS is able to achieve its experimental objectives. An internal calibration of the detectors has demonstrated charge resolution of ~0.2 charge units for stopping Fe ions. In determining the elemental abundances of ultraheavy Galactic cosmic rays, HIIS offers better resolution and a four-fold increase in statistics over the largest earlier experiment.

HIIS also offers a deep survey of space radiation which will thoroughly define the environment for the Space Station and other satellites using a 28° low altitude orbit. This survey is likely to lead to new discoveries about the radiation environment in space.

In fact, although we have so far examined less than 1% of the HIIS detector area, we have already made an unanticipated discovery: we observed Fe ions at ~600 MeV/n, well below the geomagnetic cutoff. Although the analysis is still too crude to permit any conclusions, the observed flux suggests that these ions may be partially-ionized solar energetic particles. Such particles could have significant effects on satellite electronics; they are not included in current models of the radiation environment.

ACKNOWLEDGEMENTS

REFERENCES

1.   O'Sullivan, D. et al.: The Ultra Heavy Cosmic Ray Experiment. First LDEF Post-Retrieval Symposium, NASA CP-3134, 1992.

2.   Shirk, E.K. and Price, P.B.: Charge and Energy Spectra of Cosmic Rays with $Z \geq 60$. Astrophys. J., vol. 220, 1978, pp. 719-33.

3.   Binns, W.R. et al.: Abundances of Ultraheavy Elements in the Cosmic Radiation: Results from HEAO 3. Astrophys. J. vol. 346, 1989, pp. 997-1009.

4.   Fowler, P.H. et al.: Ariel 6 Measurements of the Ultraheavy Cosmic Rays. Astrophys. J., vol. 314, 1987, pp. 739-46.

5.   Stone, E.C. et al.: The Cosmic Ray and Solar Flare Isotope Experiments in the CRRES, NOAA-I and Ulysses Satellites. in *Particle Astrophysics: The NASA Cosmic Ray Program for the 1990's and Beyond*, eds. W.V. Jones et al., AIP Conf. Proc. 203, 1989, pp. 48-57.

6.   Garcia-Munoz, M.: The Cosmic Ray and Solar Flare Isotope Experiments in the CRRES, NOAA-I and Ulysses Satellites. *ibid.*, pp. 37-43.

7.   Adams, J.H.Jr., Beahm, L.P.; and Tylka, A.J.: The Charge State of the Anomalous Component: Results from the Trapped Ions in Space Experiment (and references therein). Astrophys. J. vol. 377, 1991, pp. 292-305.

8.   Beaujean, R.; Enge, W.; and Siegmon, S.: The Resolving Cosmic Ray Experiment with Plastic Track Detectors on Spacelab 1. Proc. 16th ICRC (Kyoto), vol. 12, 1979, pp. 350-4.

9.   Singh, R.K. et al.: Ionization State of the Anomalous Cosmic Rays. Astrophys. J., vol. 374, 1991, pp. 753-63.

10. Mason, G.M.: SAMPEX Mission Overview. AIP Conf. Proc. 203, 1989, pp. 44-7.

11. Reames, D.V. et al.: The Energetic Particles: Acceleration, Composition, and Transport Experiment on the ISTP/Wind Spacecraft. *ibid.*, pp 32-6.

12. Brewster, N.R.; Frier, P.S.; and Waddington, C.J.: The Propagation of Ultraheavy Cosmic Ray Nuclei. Astrophys. J., vol. 264, 1983, pp. 324-336.

13. Chan, J.H. and Price P.B.: Composition and Energy Spectra of Heavy Nuclei of Unknown Origin Detected on Skylab. Phys. Rev. Lett., vol. 35, 1975, pp. 539-42.

14. Grigorov, N.L. et al.: The Charge State of Anomalous Oxygen of Cosmic Rays. Geomagnetism and Aeronomy, vol. 29, 1989, pp. 889-91.

15. Beaujean, R.; Jonathal, D.; and Enge, W.: Heavy Ion Measurements on LDEF. First LDEF Post-Retrieval Symposium, NASA CP-3134, 1992.

16. Adams, J.H.Jr.; Silberberg, R.; and Tsao, C.H.: Cosmic Ray Effects on Microelectronics (CREME), Part I: The Near-Earth Particle Environment. NRL Memorandum Report 4506, 1981.

17. Adams, J.H.Jr.; Letaw, J.R.; and Smart, D.F.: CREME Part II: The Geomagnetic Cutoff Effects. NRL Memorandum Report 5099, 1983.

18. Tsao, C.H. et al.: CREME Part III: Propagation of Cosmic Rays in the Atmosphere. NRL Memorandum Report 5402, 1984.

19. Adams, J.H.Jr.: CREME Part IV. NRL Memorandum Report 5901, 1986.

20. Adams, J.H.Jr. et al.: The Charge State fo the Anomalous Component. Astrophys. J. Letters, vol. 375, 1991, pp. L45-L48.

21. Luhn, A. et al.: Ionic Charge States of N, Ne, Mg, Si, and S in Solar Energetic Particle Events. Adv. in Space Res., vol. 4, 1984, pp. 161-164.

22. Breneman, H. and Stone, E.C.: Solar Coronal and Photospheric Abundances from Solar Energetic Particle Measurements. Astrophys. J., vol. 299, 1985, pp. L57-L61.

23. Oschlies, K.; Beaujean, R.; and Enge, W.: On the Charge State of Anomalous Oxygen. Astrophys. J., vol 345, 1989, pp. 776-81.

24. Biswas, S. et al.: Observation of Low-Energy (30-100 MeV nucleon^{-1}) Partially Ionized Heavy Ions in Galactic Cosmic Rays. Astrophys. J. Letters, vol. 359, 1990, pp. L5-L9.
25. Grigorov, N.L. et al.: Heavy Ions in Cosmic Rays. Nuclear Physics (Yadernaya Fizica), vol. 53, 1991, pp. 1340-5.
26. CR-39 is poly diethylene glycol bis-alyl carbonate and was invented at Pittsburgh Plate Glass's Columbia Resin Laboratory in Barberton, OH.
27. Adams, J.H.Jr.: A Curing Cycle for Detector-Quality CR-39. Nucl. Tracks: Meth., Inst. and Appl., Suppl. 3, 1982, pp. 145-148.
28. Lexan is the trade name for bis-phenol A polycarbonate, as sold by General Electric, Pittsfield MA. It is also sold under the tradenames of Tuffak and Rodyne-P.
29. Stiller, B.; Adams, J.H.Jr.; and Beahm, L.P.: Ultraviolet Enhancement of Tracks in Lexan with Black Fluorescent Lamps. Nucl. Tracks, vol. 12, 1986, pp. 137-40.
30. Kapton is a polyamide plastic manufactured by Du Pont Inc., Wilmington, DE.
31. Fleischer, R.L.; Price, P.B.; and Walker, R.M.: *Nuclear Tracks in Solids: Principles and Applications.* (Berkeley: University of California Press), 1975, pp. 57-63.
32. Benton, E.V. and Nix, W.D.: The Restricted Energy Loss Criterion for Registration of Charged Particles in Plastics. Nucl. Inst. Meth., vol. 67, 1969, pp. 343-7.
33. Henke, R.P. and Benton, E.V.: On Geometry of Tracks in Dielectric Nuclear Track Detectors. Nucl. Inst. Meth., vol. 97, 1971, pp. 483-9; Somogyi, G. and Szalay, S.A.:Track-Diameter Kinetics in Dielectric Track Detectors. Nucl. Inst. Meth., vol. 109, 1973, pp. 211-32.
34. Adams, J.H.Jr.: Automated Track Measurements in CR-39. Nucl. Tracks, vol. 4, 1980, pp. 67-76.
35. O'Sullivan, D.; Thompson, A.; and Fowler, P.H.: The Abundance of Actinide Elements in the Galactic Cosmic Radiation. Nucl. Tracks Radiat. Meas., vol. 11, 1986, pp. 95-85.
36. O'Sullivan, D. and Thompson, A.: The Observation of a Sensitivity Dependence on Temperature during Registration in Solid State Nuclear Track Detectors. Nucl. Tracks, vol. 4, 1980, pp. 271-76.
37. Thompson, A. et al.: The Dependence of Track Response on Registration Temperature in Lexan and CR-39. Nucl. Tracks: Meth., Inst. and Appl., Suppl. 3, 1982, pp. 171-4.
38. O'Sullivan, D. et al.: New Results on the Investigation of the Variation of Nuclear Track Detector Response with Temperature. Nucl. Tracks and Radiat. Meas., vol. 8, 1984, pp. 143-6.
39. Adams, J.H.Jr. and Beahm, L.P.: The Registration Temperature Effect for Lightly Ionizing Particles in CR-39. Nucl. Tracks, vol. 12, 1986, pp. 387-90.
40. Berrios, W.M.: LDEF Post-Flight Thermal Analysis: Orbital Thermal Environment Data Package. NASA/LaRC, Hampton, VA; and Use of LDEF Thermal Measurement System for Verification of Thermal Models. First LDEF Post-Retrieval Symposium, NASA CP- 3134, 1992.

41. Adams, J.H.Jr. and Beahm, L.P.: A Study of Long Term Thermal Annealing on Lexan Plastic Track Detector. Nucl. Tracks: Meth. Inst. and Appl., Suppl. 3, 1982, pp. 145-148.
42. Henke, R.P.; Benton, E.V.; and Heckman, H.H.: Sensitivity Enhancement of Plastic Nuclear Track Detectors Through Photo-oxidation. Rad. Eff., vol. 3, 1970, pp. 43-49.
43. Price, P.B. and Drach, J.: Dependence of Response of Plastic Track Detectors on Post-Irradiation Aging Time, Temperature, and Atmosphere. Nucl. Inst. Meth., vol. B28, 1987, pp. 275-9.
44. Domingo, C. et al.: Latent Track Intensification Due to Ageing in Solid State Nuclear Track Detectors. Nucl. Tracks and Radiat. Meas., vol. 15, 1988, pp. 47-50.; The Influence of Latent Track Variations on Ultra Heavy Nuclei Identification with Solid State Nuclear Track Detectors. Proc. 21st ICRC (Adelaide), vol. 4, 1990, pp. 437-40.
45. Yadav, J.S. and Singh, R.K.: Change of CR-39(DOP) Track Detector Response as a Result of Space Exposure. Nucl. Tracks Radiat. Meas., vol. 17, 1990, pp. 579-82.
46. Drach, J. et al.: Effect of Oxygen on Response of Plastic and Glass Track Detectors. Nucl. Inst. Meth., vol. B28, 1987, pp. 364-8.
47. Bevington, P.R.: *Data Reduction and Error Analysis for the Physical Sciences.* (New York: McGraw-Hill), 1969, pp. 313-6.
48. McGuire, R.E.; Von Rosenvinge, T.T.; and McDonald, F.B.: The Composition of Solar Energetic Particles. Astrophys. J. vol. 301, 1986, pp. 938-61.
49. Mason, G.M.: The Composition of Galactic Cosmic Rays and Solar Energetic Particles. Rev. Geophys., vol. 25, 1987, pp. 685-96.